Developing a 3D-Printed Parallel Manipulator for Enhancing Robotics Education

Hentai DAI
Faculty of Engineering,
University of Nottingham
Nottingham, UK
ezxhd1@nottingham.ac.uk

Xi WANG
Faculty of Engineering,
University of Nottingham
Nottingham, UK
ezzxw5@exmail.nottingham.ac.uk

Adam CROWE
Faculty of Engineering,
University of Nottingham
Nottingham, UK
egyac1@exmail.nottingham.ac.uk

Xin DONG
Faculty of Engineering,
University of Nottingham
Nottingham, UK
ezzxd@exmail.nottingham.ac.uk

Gang CHEN
College of Information Science and Engineering
Jiaxing University
Jiaxing 314001, China
6450949@qq.com

2024 29th International Conference on Automation and Computing (ICAC) | 979-8-3503-6088-2/24/$31.00 ©2024 IEEE | DOI: 10.1109/ICAC61394.2024.10718795

***Abstract*—: This paper presents a specific parallel manipulator model known as the 3-RSR wrist for enhancing educational accessibility for students pursuing robotics. Fabricated using 3D printing to ensure affordability and accessibility, the manipulator is introduced as a cost-effective educational tool, with a replication cost of £85.76 for students. The control system was implemented successfully and underwent optimization for improved performance. An in-depth analysis of the 3-RSR wrist's mechanical configuration, control, kinematics and workspace capabilities is provided in this paper. The manipulator achieves a high degree of accuracy in its operational limits, closely mirroring those of geometry limits with 99.5% accuracy and reaching 95% accuracy in comparison to theoretical limits.**

Keywords—Parallel manipulator, parallel mechanism, 3-RSR wrist, kinematic modelling, workspace analysis.

I. INTRODUCTION

A parallel manipulator is a mechanical system composed of a mobile platform, called an end-effector, connected to a fixed base by a set of parallel kinematic chains, called limbs. Having the limbs connected in parallel rather than in series provides manipulators with high precision, high load capacity, high rigidity, and high speed but with a small workspace [1]. The most well-known parallel manipulator is the Stewart Platform, which has six identical limbs and is commonly used for flight simulators and machine tools [2]. Parallel manipulators are characterised by the end-effector's rotational and translational Degrees of Freedom (DoF). Generally, the more DoF a parallel manipulator has, the more complicated and expensive the design and control becomes

The 3-RSR wrist is a type of parallel mechanism that typically consists of three limbs connecting the base to the moving platform. Each limb is configured in a Revolute-Spherical-Revolute (RSR) sequence of joints. The 3-RSR wrist has two rotational and one translational DoF [3]. The wrist allows the end-effector to rotate about the x-axis, rotate about the y-axis and translate along the z-axis. The 3-RSR parallel robotic manipulator is thus characterized by its three RSR-configured limbs that support and move the end effector. The specific configuration of joints and the parallel nature of the manipulator offer a unique combination of advantages in terms of control, stability, and range of motion.

Fig. 1. The developed 3-RSR wrist

Using a 3-RSR wrist as a teaching tool in robotic education presents several advantages, particularly because of its unique structure and characteristics. It allows students to explore complex kinematic concepts tangibly. Unlike serial manipulators, parallel robots offer a direct way to understand the principles of parallel kinematics, including issues related to stiffness, stability, and precision. Also, working on a 3-RSR manipulator offers hands-on experience in assembling, programming, and troubleshooting robotic systems, crucial skills for any robotics student.

The focus of this study is to make parallel manipulators more accessible to robotics students, facilitating them to learn mechanical design, kinematics, workspace, and control of parallel manipulators. A type of parallel manipulator called the 3-RSR wrist was developed. The wrist was designed so that it can be easily manufactured by students, as this will enable them to get hands-on experience. The manufacturing process used is Fused Deposition Modelling (FDM) 3D Printing, as the machines for this process are becoming increasingly common at both Universities and within homes.

The rest of this paper is structured as follows: Section II reviews related work on parallel manipulators. Section III describes the overall system of the 3-RSR wrist, including the mechanism of the 3-RSR wrist, actuation and control, and fabrication and materials. Section IV presents the kinematics analysis of the 3-RSR wrist. In Section V, the workspace analysis with validation is presented. Finally, Section VI concludes this study and presents future work.

II. Related Works

Parallel manipulators or parallel mechanisms have a wide range of applications, such as robot grasping [4], surgical robots [5]and haptic feedback [6] [7]. For example, Bazman et al., [5] developed a parallel robot that utilises a 3-RSR wrist to develop a surgical robot. This wrist can pitch and yaw by 90°, providing the robot with more manoeuvrability than a surgeon's hand while being less invasive. The 3-RSR wrist's capabilities also extend to the development of a wearable haptic feedback device [7] , advancing virtual reality technologies. The Stewart platform and Delta robot have historically dominated research in this field, especially in the realm of machine tools. Researchers at the University of Nottingham developed a series of walking machine tools [8] [9] derived from the Stewart platform, alongside a parallel manipulator aimed at enhancing cooperative continuum robots [10]. Notably, Axinte et al., [11] developed a robotized machine tool, Mini-RoboMach, consisting of a walking hexapod robot, which is similar to the Stewart platform, and a slender continuum arm. This fusion enables versatile, in-situ tasks like repairs in environments that are otherwise challenging or dangerous to access. Besides of Stewart platform, the growing robotics industry signals an expanding interest and application base for the 3-RSR wrist [12]. The 3-RSR wrist, characterized by its 2R1T Degrees of Freedom (DoF), plays a pivotal role in expanding tool workspaces [13]. Key explorations into forward and inverse kinematics of the parallel mechanisms [14] [15] have laid foundational insights, though its design, control mechanisms, and optimization method [16] await further exploration.

III. System Configuration

A. Mechanism of the 3-RSR wrist

The 3-RSR wrist is composed of three identical limbs, each incorporating a sequence of revolute, spherical, and another revolute joints. A revolute joint allows rotation about one axis, while a spherical joint allows rotation about three axes. Each limb is comprised of a lower linkage and an upper linkage, the two linkages are connected by a spherical joint. The lower linkage connects to a motor shaft at the end opposite the spherical joint as the first revolute joint. The upper linkage connects to the end effector at the end opposite the spherical joint as the second revolute joint. The mechanical design of the 3-RSR wrist is shown in Fig. 2.

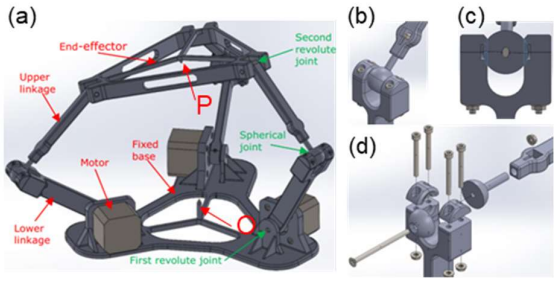

Fig. 2. Mechanical design of the 3-RSR wrist. (a) CAD model of the 3-RSR wrist. (b) Isometric view of the spherical joint. (c) Contact surface of the spherical joint. (d) Exploded view of the spherical joint

The wrist is actuated by three stepper motors, each of which is fastened to the fixed base. Each lower linkage is fastened to its motor shaft by a grub screw, this is the first revolute joint. Every lower linkage connects to its upper linkage by a spherical joint (see Fig. 2(b)-(c)). Each upper linkage is connected to the end-effector by a pivot pin, which is the second revolute joint (see Fig. 2(d)). The upper linkage sits in a gap in the end-effector. The gap stops the axial movement of the linkage, while it can rotate freely about the pin. The pivot pins are fastened to the end-effector by a grub screw. Because of the precision of 3D printing, the interference fit between the parts is also a factor to be considered in the design. The first set of revolute joints was designed to have an adequate interference fit, while the spherical joints have an inadequate clearance fit because they have 1mm of excess play. The second set of revolute joints has an adequate clearance fit with the pivot pin, but the clearance fit with the end-effector allows 0.5mm of excess play. In addition, a pin was added to the centre of both the end-effector and fixed base. The tip of these pins represents the kinematic points P and O, as marked in Fig. 2(a). The two pins facilitate the accuracy testing of the wrist's end effector.

B. Actuation and Control

The parallel manipulator is actuated by 3 stepper motors (NEMA-17) controlled by an Arduino Uno microcontroller and driven by three motor drivers (A4988), which are powered by a DC power supply (Fig.3). Based on the controller program, the microcontroller outputs a HIGH or LOW signal to pins on the motor drivers. The motor drivers determine whether each motor is ON or OFF when to step, and what direction to step in. The stepper motors rotate with a discrete step size of 1.8°/step, this can be reduced by using micro-stepping. The microcontroller determines a micro-stepping value of 1, 2, 4 or 8; a micro-stepping value of 4 would reduce the step size to 0.45°/step. The stepper motors require a current greater than what the microcontroller can deliver, so a DC power supply is connected to the motor drivers which is then supplied to the motors.

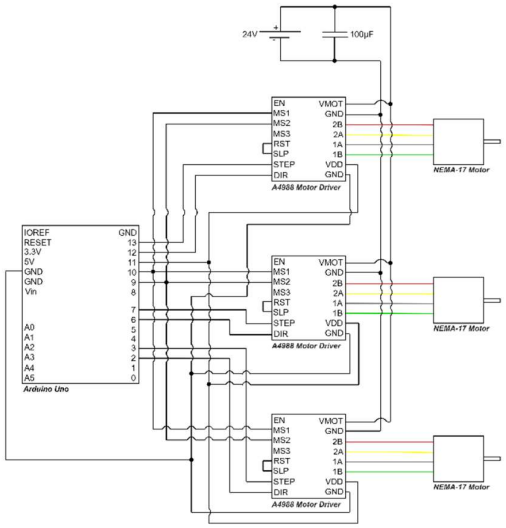

Fig. 3. Control circuit diagram

A motor angle will have a continuous value (θn), but the motor moves in discrete steps. The motor angle must be approximated to the closest step position (σn), and then the motor can be actuated by a discrete number of steps (sn). Increasing the micro-stepping value will create a more accurate approximation of the motor angle. Considering the step size of 1.8°/step and that when the motors are off θn = 161, the approximated step position is

$$\sigma_n = round\left[(\theta_n - 161) \times \frac{micro-steppin\ \ valve}{1.8}\right] \quad (1)$$

C. Fabrication and materials

The components of the manipulator were designed to be manufactured using an FDM 3D Printer(i.e., Ultimaker 2+ [17]), as this is an accessible manufacturing technique. The dimensions for the end-effector/base radius (D) and linkage length (L) can be easily adjusted within the CAD model. Adjusting these dimensions changes the workspace and allows the user to ensure the parts are small enough to be manufactured on their machine. The material used was PLA as this is the most common material for FDM printers and it is easy to print with.

The spherical joint's contact surface has a major impact on the smoothness and accuracy of the wrist's motion. The spherical joint has to rotate about three axes, compared to the revolute joints rotating about one. The spherical joint is the limiting factor for the wrist's maximum rotation about the x and y-axis, and it is likely the weakest part of the wrist. Thus, it is essential to find the optimal balance between the spherical joint's strength and range of motion, while ensuring it can be 3D printed with an acceptable contact surface. The problem of surface roughness can be solved by printing the spherical surfaces in two halves, removing the need for support structures, and then sanding down the contact surfaces. The contact surfaces were moved as close to the edge of the joint as possible, to maximise the range of motion, but they were not moved so far out that the joint was not adequately supported. For the spherical joints, the layer height of the 3D printing is the finest one, 0.06mm, printed by a 0.2mm nozzle. For other structural parts, the layer height is 0.2mm, printed by a 0.4mm nozzle. The infill of the spherical joints and other parts is 80% and 40%, respectively. Other printing parameters are set to default.

The total cost for a student to replicate this project's 3-RSR wrist is £85.76, as shown in Table I. If the student already has the electronic components, the cost for the 3D printed parts and hardware is £14.73. The 3D printed 3RSR wrist is highly cost-effective compared to similar educational delta robotic platforms such as the DFRobot 4-DOF Robot Arm Kit (£150 - £200)[18], Makeblock Ultimate Robot Kit (£300 - £350)[19] and He3D K280 Delta 3D Printer (£400)[20]. While these platforms offer various features and extensive educational resources, the 3D-printed 3RSR wrist provides significant savings and learning opportunities in parallel kinematics, control systems, and 3D printing.

TABLE I. COST AND QUANTITY OF PARTS AND MATERIALS

Item	*Quantity*	*Cost*
Arduino Uno	1	£23.00
Breadboard	1	£3.00
Motor Driver	1	£9.00
Stepper Motor	3	£36.00
M3 Threaded Insert	6	£0.12
M3 Washer	15	£0.30
M3 50mm Countersunk Bolt	3	£0.12
M3 30mm Bolt	12	£1.80
M3 Nut	15	£0.75
M3 12mm Countersunk Bolt	12	£0.48
M3 6mm Grub Screw	6	£0.36
5mm Dowel Pin	3	£0.48
300g PLA Filament	1	£10.32
100uF Decoupling Capacitor	3	£0.03
Total		£85.76

IV. KINEMATICS ANALYSIS

Kinematics describes how a rigid body moves; it considers position, velocity, and acceleration, but does not consider forces. Forward kinematics relates the motor angles (θ_1, θ_2, θ_3) to the coordinates of the end effector (h, θ_x, θ_y), and inverse kinematics does the opposite. The end-effector coordinates can also be found in the cartesian coordinate system (P_x, P_y, P_z). Inverse kinematics is the most useful for parallel manipulators, but it often produces multiple solutions for joint positions. If a joint reaches its limit or multiple joints align collinearly, a singularity occurs, an issue which causes the robot to lose a degree of freedom. The kinematics allows the manipulator to be controlled and it can also be used to analyse the end-effector's workspace.

A. Inverse Kinematics

The lower linkage and upper linkage have the same length, $L = |B_nA_n| = |B_nC_n|$. The end effector and fixed base both have the same radius, $D = |A_nO| = |C_nP|$. This geometrical symmetry means the upper half of the wrist has the same geometry as the lower half, except its orientation and position differ; there is a plane of symmetry through the spherical joints (see Fig. 4(a)). Each limb is offset about the z-axis by an angle ϕ. The inverse kinematics are derived by solving the kinematic chain for one limb. The first revolute joint lies at a distance, D, from the centre of the fixed base, $\overline{AO}_n$. The spherical joint moves along an arc, at a distance L from the first revolute joint, $\overline{BA}_n$.

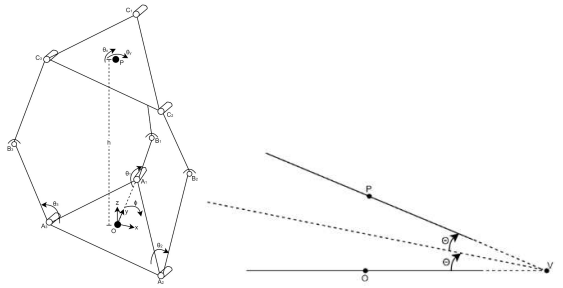

Fig. 4. Schematic diagram of (a) 3-RSR wrist kinematic model. (b) Kinematic model of plane's A, B and C

The position of the spherical joint can be found in terms of the motor angle θ_n:

$$\overline{BO}_n = \overline{AO}_n + \overline{BA}_n \quad (2)$$

$$\overline{BO}_n = \begin{bmatrix} D\sin\emptyset_n \\ D\cos\emptyset_n \\ 0 \end{bmatrix} + \begin{bmatrix} -L\cos\theta_n\sin\emptyset_n \\ -L\cos\theta_n\cos\emptyset_n \\ L\sin\theta_n \end{bmatrix} \quad (3)$$

If the upper half of the wrist has not been rotated, the symmetry with the lower half means that Eq. (3) can be reoriented, to find:

$$\overline{PB'}_n = \begin{bmatrix} -L\cos\theta_n\sin\emptyset_n - D\sin\emptyset_n \\ -L\cos\theta_n\cos\emptyset_n - D\cos\emptyset_n \\ L\sin\theta_n \end{bmatrix} \quad (4)$$

Quaternions are an extension of complex numbers; the one real part represents a rotation magnitude, and the three imaginary parts represent the axis of rotation. The upper half of the wrist will be rotated about the x and y-axis, each of these rotations can be represented in quaternion form as:

$$q_x = \cos\frac{\theta_x}{2} + \sin\frac{\theta_x}{2}\hat{\imath} = c_x + s_x\hat{\imath} \quad (5)$$

$$q_y = \cos\frac{\theta_y}{2} + \sin\frac{\theta_y}{2}\hat{\jmath} = c_x + s_x\hat{\jmath} \quad (6)$$

Using Eq. (4) - (6), once the upper half of the wrist has been rotated about the x and y-axis, the vector going from the spherical joint to the centre of the fixed base can be found after rotation:

$$\overline{PB}_n = (q_y q_x)\overline{PB'}_n(\overline{q_y q_x}) \quad (7)$$

To complete the kinematic chain, the vector going from the centre of the fixed base to the centre of the end-effector can be found, by using Eq. (3) and (7):

$$\overline{PO} = \overline{PB}_n + \overline{BO}_n \quad (8)$$

$$\overline{PO} = \begin{bmatrix} -2es_y^2c_x^2 + 2fc_yc_xs_ys_x + 2gc_ys_yc_x^2 \\ 2ec_yc_xs_ys_x - 2fc_y^2s_x^2 - 2gc_y^2s_xc_x \\ -2ec_yc_x^2s_y + 2fc_y^2c_xs_x + 2g(1 - c_y^2s_x^2 - s_y^2) \end{bmatrix} \quad (9)$$

The z-component of the vector PO is equal to the end-effector coordinate h. To get this equation in terms of the motor angle, θ_n, some intermediate variables p, q and r, are introduced. The intermediate variables are in terms of the end-effector coordinates (h, θ_x, θ_y),

$$p = q\sin\theta_n + r\cos\theta_n \quad (10)$$

$$p = h - 2D\sin\emptyset_n\, c_yc_x^2s_y + 2D\cos\emptyset_n\, c_y^2c_xs_x \quad (11)$$

$$q = 2L(1 - c_y^2s_x^2 - s_y^2) \quad (12)$$

$$r = 2L(-\sin\emptyset_n\, c_yc_x^2s_y + \cos\emptyset_n\, c_y^2c_xs_x) \quad (13)$$

Using trigonometric identities and rearranging, Eq. (10) can be used to find the motor angles θ_n (for n = 1,2,3). This equation for the motor angle is in terms of the intermediate variables, which are in terms of the end-effector coordinates,

$$\theta_n = 180 - \sin^{-1}\left(\frac{p}{\sqrt{q^2+r^2}}\right) + \sin^{-1}\left(\frac{r}{\sqrt{q^2+r^2}}\right) \quad (14)$$

The inverse position kinematics have been solved and verified using a SOLIDWORKS model. Eq. (5), (6), (11) - (14) find the motor angles. Eq. (9) then allows the end-effector position to be converted from the original coordinate system to the cartesian coordinate system.

B. Forward Kinematics

The first set of revolute joints lies on plane A, while the second set of revolute joints lies on plane C. The symmetry between the upper and lower half of the wrist means there is a plane of symmetry between the two halves, on which the spherical joints lie, plane B. The centre of the end-effector, P, is the centre of the fixed base, O, rotated by 2Θ about the point V (see Fig. 4(b)) The first set of revolute joints and the origin, O, all lie on a flat plane, so the equation for plane A is z = 0. The origin lies within plane A, so the vector normal to plane A is

$$\bar{n}_A = 0\hat{\imath} + 0\hat{\jmath} + w\hat{k} \quad (15)$$

The vector normal to plane B can be found from the cross product of two vectors going between the various spherical joints,

$$\bar{n}_B = \overline{B_2B_3} \times \overline{B_2B_1} = a\hat{\imath} + b\hat{\jmath} + c\hat{k} \quad (16)$$

, where a, b and c can be found using Eq. (3):

$$a = -2L\sin\left(\frac{\theta_3-\theta_2}{2}\right)\left[L\sin\left(\frac{\theta_3+\theta_2}{2}\right)\sin\left(\frac{\theta_1-\theta_2}{2}\right)\cos\left(\frac{\theta_1+\theta_2}{2}\right) + (1.5D - L\cos\theta_1 - 0.5L\cos\theta_2)\cos\left(\frac{\theta_3+\theta_2}{2}\right)\right] \quad (17)$$

$$b = -\sqrt{3}L\left[2\left(-D + L\cos\left(\frac{\theta_3+\theta_2}{2}\right)\cos\left(\frac{\theta_3-\theta_2}{2}\right)\right)\sin\left(\frac{\theta_1-\theta_2}{2}\right)\cos\left(\frac{\theta_1+\theta_2}{2}\right) + (D - L\cos\theta_2)\sin\left(\frac{\theta_3-\theta_2}{2}\right)\cos\left(\frac{\theta_3+\theta_2}{2}\right)\right] \quad (18)$$

$$c = \sqrt{3}L[(1.5D - L\cos\theta_1 - 0.5L\cos\theta_2)\left(-D + L\cos\left(\frac{\theta_3+\theta_2}{2}\right)\cos\left(\frac{\theta_3-\theta_2}{2}\right) + \frac{1}{2}\mathrm{L}(-D + L\cos\theta_2)\sin\left(\frac{\theta_3+\theta_2}{2}\right)\cos\left(\frac{\theta_3-\theta_2}{2}\right)\right)] \quad (19)$$

The equation for plane B has the form:

$$ax + by + cz + d = 0 \quad (20)$$

, where the coefficient d can be found by substituting the vector for the first spherical joint, $\overline{BO_1}$, into Eq. (20).

Using Eq. (15) and (16), the dot product of the vectors normal to plane A and B, can be rearranged to find the angle between these planes,

$$\Theta = \cos^{-1}\left(\frac{\bar{n}_A\cdot\bar{n}_B}{|\bar{n}_A||\bar{n}_B|}\right) = \cos^{-1}\left(\frac{c}{\sqrt{a^2+b^2+c^2}}\right) \quad (21)$$

The axis u lies where planes A and B intersect, point V lies on this axis. Applying z = 0 to Eq. (20) and setting x to be a free parameter, t, results in the equation for the axis,

$$u = \begin{bmatrix} 0 \\ -d/b \\ 0 \end{bmatrix} + \begin{bmatrix} 1 \\ -a/b \\ 0 \end{bmatrix} t \quad (22)$$

Point V lies on the axis u such that:

$$\overline{OV} = \begin{bmatrix} 0 \\ -d/b \\ 0 \end{bmatrix} \quad (23)$$

Rodrigues' rotation formula is a method for finding a rotation matrix, which represents a rotation about an axis. When a vector is multiplied by a rotation matrix, it gives the vector after rotation. Rodrigues' rotation formula, $[R]$, will be applied to represent a clockwise rotation of 2Θ radians about axis $\hat{u}$. Using the rotation formula on the vector in Eq. (23) results in:

$$\overline{PV} = [R]\overline{OV} = \begin{bmatrix} \frac{d}{b}u_x u_y(-2q^2+2) \\ \frac{d}{b}[(2q^2-1)u_y^2(-2q^2+2)] \\ \frac{d}{b}u_x(-2q\sin\theta) \end{bmatrix} \quad (24)$$

, where $q = c/(\sqrt{a^2+b^2+c^2})$.

Using the origin, O, as the reference frame, the cartesian coordinates for the end-effector can be found:

$$\overline{PO} = \overline{PV} - \overline{OV} = \begin{bmatrix} \frac{d}{b}u_x u_y(-2q^2+2) \\ \frac{d}{b}[(u_y^2-1)(-2q^2+2)] \\ \frac{d}{b}u_x(-2q\sin\theta) \end{bmatrix} \quad (25)$$

The forward position kinematics have been solved for the end-effector position in the cartesian coordinate system (P_x, P_y, P_z) The equations have been verified using a SOLDIWORKS model and by comparing to inverse kinematics results.

V. Workspace Analysis and Validation

A. Workspace Analysis

Analysing the workspace allows the wrist to be optimised by increasing the end-effector's range of motion. A set of constraints is required to determine the wrist's allowable workspace. The constraints come from both the limitations of the wrist geometry and kinematic equations. The end-effector limits found from the CAD model can be converted to motor angles using the inverse kinematics, and then to cartesian coordinates using the forward kinematics. Using the CAD model of the wrist, the possible range of end-effector coordinates (h, θx, θy) can be found. The end-effector is at its maximum height of $2L$, when all three limbs are vertical. The minimum height is limited by the geometry of the spherical joint (see Fig. 5), reducing the length of each linkage will reduce the minimum height. The maximum rotation about the x and y-axis, in both the positive and negative directions, is limited by the geometry of the spherical joint (see Fig. 5(a) and 5(b)). The θx and θ_y limits are determined by the ratio of D/L, decreasing this ratio increases the end-effector's rotation limits.

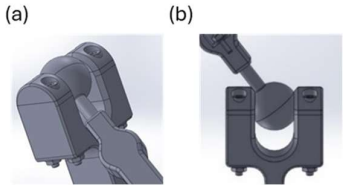

Fig. 5. Geometry constrains of the spherical joint.

Using the above constraints derived from the geometry and kinematic analysis, the workspace was mapped out in the cartesian coordinate system using MATLAB (see Fig. 6). For each end-effector coordinate, 200 values were used, incrementally spaced between the coordinate's maximum and minimum value. The top-down view of the workspace map shows the first six outermost coordinates, as shown in Fig. 6(b). The symmetry about the first, third, and fifth coordinates can be seen in this view.

TABLE II. Comparison of Limits Found from the CAD Model to the Workspace Map

CAD model (mm)			*Workspace map (mm)*			*Difference (mm)*		
p_x	p_y	p_z	p_x	p_y	p_z	p_x	p_y	p_z
0	69.8	174.5	0	68.5	176	0	-1.3	1.5
55.5	32.1	126.2	55.4	33.7	126	-0.1	1.6	-0.2
60.1	-34.7	174.5	59.9	-34.5	174	-0.2	0.2	-0.5
0	-65.3	129.3	0	-65.0	129	0	0.3	-0.3
-60.1	-34.7	174.5	-59.9	-34.5	174	0.2	0.2	-0.5
-55.5	32.1	126.2	-59.4	33.7	126	0.1	1.6	-0.2
0	0	78.1	0	0	78.2	0	0	0.1
0	0	240	0	0	239.7	0	0	-0.3

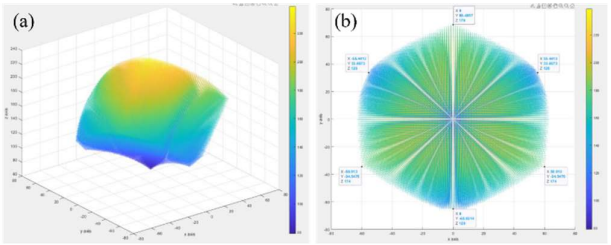

Fig. 6. Workspace map by MATLAB. (a) Isometric view. (b) Top view

The limits of the workspace map were compared to the limits found in the CAD model. The results shown in Table II indicate an error of 0.5% for end-effector positions near the edges of the map, while the bulk of the workspace map is accurate. Fig.7 shows the wrist at three points while moving between the limits in Table II. The motors have an angle resolution of 0.45°, using the forward position kinematics, the end-effector has a resolution of 1.9mm. The play in the end-effector means the wrist has an inaccuracy of 6mm. The minimum end-effector distance is 78.1mm, by combining the resolution and inaccuracy, the actual end-effector position will be within 90-110% of the target end-effector position.

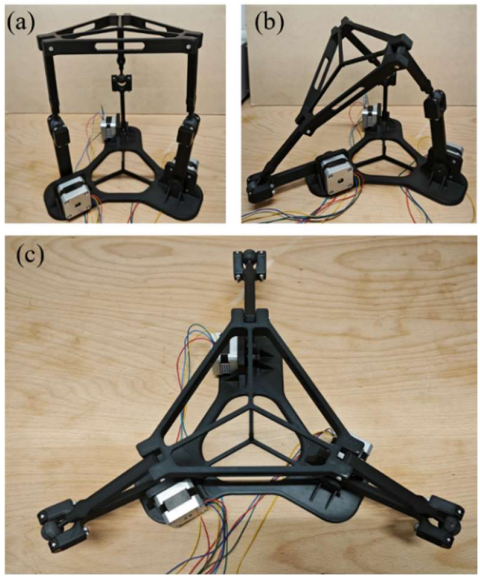

Fig. 7. The wrist at three points within the limits in Table II

B. Experiment and Validation

While the motors were not powered, the mechanical limits of the end-effector were measured and compared to the theoretical limits. For each limit, five readings were taken from different viewing angles, to minimize parallax error. Any anomalous results were discarded, and then the readings were

averaged. The observed limits had an accuracy of 95% compared to the theoretical limits (see Table III). Play in the spherical joints and second set of revolute joints, allowed the wrist to sag.

TABLE III. THEORETICAL AND OBSERVED MECHANICAL LIMITS OF THE WRIST

Limit	*Theoretical value*	*Observed value*	*Error*
Maximum height	240.0 mm	239.0 mm ± 0.5	0.04%
Minimum height	78.1 mm	75.2 mm ± 0.5	4%
Maximum rotation about the x-axis	53.0°	54.5° ± 0.5	3%
Minimum rotation about the x-axis	-43.6°	-45.8° ± 0.5	5%

Furthermore, the performance of the 3-RSR wrist underload was tested. The end-effector was loaded with masses up to 1.5kg and the height was recorded at each weight. At each weight, three readings were taken and averaged. The results were plotted (see Fig. 8), and the gradient provides the stiffness of the wrist, which is 470N/m±25.

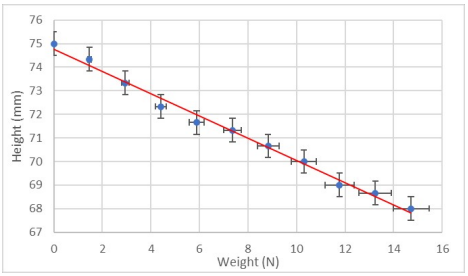

Fig. 8. Height of the end-effector at various loads

VI. CONCLUSION AND FUTURE WORK

In this paper, we present the design, fabrication, kinematics and workspace analysis of a 3-RSR parallel manipulator, making parallel manipulators more accessible to robotics education. The fabrication and assembly of the wrist were completed successfully at a cost of £85.76. The control system effectively executed the parallel motion, accurately determining the optimum micro-stepping value and maximum stepping rate. The performance of the end-effector was qualitatively as expected, indicating successful implementation of the design and control used. Through extensive workspace analysis, we achieved a 99.5% accuracy rate in mapping the manipulator's operational boundaries as compared to its geometry limits. The observed limits were 95% accurate compared to the theoretical limits.

Future works will focus on refining the kinematic and dynamic models of the 3-RSR wrist to enhance its precision and operational efficiency. Efforts will be made to address the limitations identified in the current prototype, such as the mechanical play in joints. Additionally, the manipulator will be introduced into teaching sessions to evaluate its effectiveness in augmenting students' understanding of robotics knowledge and hands-on skills.

REFERENCES

[1] F. Pierrot, V. Nabat, O. Company, S. Krut, and P. Poignet, 'Optimal Design of a 4-DOF Parallel Manipulator: From Academia to Industry', *IEEE Transactions on Robotics*, vol. 25, no. 2, pp. 213–224, Apr. 2009, doi: 10.1109/TRO.2008.2011412.

[2] B. Dasgupta and T. S. Mruthyunjaya, 'The Stewart platform manipulator: a review', *Mechanism and Machine Theory*, vol. 35, no. 1, pp. 15–40, Jan. 2000, doi: 10.1016/S0094-114X(99)00006-3.

[3] R. Di Gregorio, 'Inverse position analysis, workspace determination and position synthesis of parallel manipulators with 3-RSR topology', *Robotica*, vol. 21, no. 6, pp. 627–632, 2003, doi: 10.1017/S0263574703005174.

[4] Z. Lu *et al.*, 'Visual-Tactile Robot Grasping Based on Human Skill Learning From Demonstrations Using a Wearable Parallel Hand Exoskeleton', *IEEE Robotics and Automation Letters*, vol. 8, no. 9, pp. 5384–5391, Sep. 2023, doi: 10.1109/LRA.2023.3295296.

[5] M. Bazman, N. Yilmaz, and U. Tumerdem, 'Dexterous and back-drivable parallel robotic forceps wrist for robotic surgery', in *2018 IEEE 15th International Workshop on Advanced Motion Control (AMC)*, Mar. 2018, pp. 153–159. doi: 10.1109/AMC.2019.8371079.

[6] H. Dai, Z. Lu, C. Yang, and S. Dai, 'A 3-DOF Haptic Feedback System for Displaying Sliding and Torsion Effects Detected by TacTip Sensor', in *2023 28th International Conference on Automation and Computing (ICAC)*, Sep. 2023, pp. 1–6. doi: 10.1109/ICAC57885.2023.10275181.

[7] D. Leonardis, M. Solazzi, I. Bortone, and A. Frisoli, 'A wearable fingertip haptic device with 3 DoF asymmetric 3-RSR kinematics', in *2015 IEEE World Haptics Conference (WHC)*, Jun. 2015, pp. 388–393. doi: 10.1109/WHC.2015.7177743.

[8] J. Camacho-Arreguin, M. Wang, X. Dong, and D. Axinte, 'A novel class of reconfigurable parallel kinematic manipulators: Concepts and Fourier-based singularity analysis', *Mechanism and Machine Theory*, vol. 153, p. 103993, Nov. 2020, doi: 10.1016/j.mechmachtheory.2020.103993.

[9] J. I. Camacho-Arreguin, M. Wang, M. Russo, X. Dong, and D. Axinte, 'Novel Reconfigurable Walking Machine Tool Enables Symmetric and Nonsymmetric Walking Configurations', *IEEE/ASME Transactions on Mechatronics*, vol. 27, no. 6, pp. 5495–5506, Dec. 2022, doi: 10.1109/TMECH.2022.3183689.

[10] M. Russo, N. Sriratanasak, W. Ba, X. Dong, A. Mohammad, and D. Axinte, 'Cooperative Continuum Robots: Enhancing Individual Continuum Arms by Reconfiguring Into a Parallel Manipulator', *IEEE Robotics and Automation Letters*, vol. 7, no. 2, pp. 1558–1565, Apr. 2022, doi: 10.1109/LRA.2021.3139371.

[11] D. Axinte *et al.*, 'MiRoR—Miniaturized Robotic Systems for Holistic In-Situ Repair and Maintenance Works in Restrained and Hazardous Environments', *IEEE/ASME Transactions on Mechatronics*, vol. 23, no. 2, pp. 978–981, Apr. 2018, doi: 10.1109/TMECH.2018.2800285.

[12] M. Hagele, 'Robots Conquer the World [Turning Point]', *IEEE Robotics & Automation Magazine*, vol. 23, no. 1, pp. 120–118, Mar. 2016, doi: 10.1109/MRA.2015.2512741.

[13] H. Fang, T. Tang, Z. He, Y. Liu, and J. Zhang, 'A novel hybrid machine tool integrating a symmetrical redundantly actuated parallel mechanism: Design, kinematics, prototype and experiment', *Mechanism and Machine Theory*, vol. 176, p. 105013, Oct. 2022, doi: 10.1016/j.mechmachtheory.2022.105013.

[14] J. Yu, X. Dong, X. Pei, and X. Kong, 'Mobility and Singularity Analysis of a Class of Two Degrees of Freedom Rotational Parallel Mechanisms Using a Visual Graphic Approach', *Journal of Mechanisms and Robotics*, vol. 4, no. 041006, Sep. 2012, doi: 10.1115/1.4007410.

[15] X. Dong, J. Yu, B. Chen, and G. Zong, 'Geometric approach for kinematic analysis of a class of 2-DOF rotational parallel manipulators', *Chinese Journal of Mechanical Engineering*, vol. 25, no. 2, pp. 241–247, Mar. 2012, doi: 10.3901/CJME.2012.02.241.

[16] Z. Lu, N. Wang, and C. Yang, 'A novel iterative identification based on the optimised topology for common state monitoring in wireless sensor networks', *International Journal of Systems Science*, vol. 53, no. 1, pp. 25–39, Jan. 2022, doi: 10.1080/00207721.2021.1936275.

[17] 'UltiMaker 2+ Connect', UltiMaker. Accessed: Jul. 09, 2024. [Online]. Available: https://ultimaker.com/3d-printers/s-series/ultimaker-2-connect/

[18] 'Desktop 5-DOF Robotic Arm Kit, High-torque Serial Servo Based On ESP32 (US Plug)', RobotShop UK. Accessed: Jul. 09, 2024. [Online]. Available: https://uk.robotshop.com/products/desktop-5-dof-robotic-arm-kit-high-torque-serial-servo-based-on-esp32-us-plug

[19] 'Makeblock mBot Ultimate: 10-in-1 Robot Building Kit for Students', Makeblock. Accessed: Jul. 09, 2024. [Online]. Available: https://www.makeblock.com/products/buy-mbot-ultimate

[20] 'HE3D K280 Large Delta 3D Printer Kit', 3DPrintersBay. Accessed: Jul. 09, 2024. [Online]. Available: https://www.3dprintersbay.com/he3d-k280-large-delta-3d-printer-kit